Simulation of the shielding of dust particles in low pressure glow discharges

Seung J. Choi and Mark J. Kushner
University of Illinois, Department of Electrical and Computer Engineering, 1406 W. Green Street, Urbana, Illinois 61801

(Received 25 November 1992; accepted for publication 4 March 1993)

The dynamics of the shielding of particulates ("dust") in low pressure glow discharges have been investigated with a pseudoparticle-in-cell simulation for electrons and ions in the vicinity of a dust particle. The potential of the dust particle, and the orbital nature of ions around the dust particle, depend on the collisionality of the ions. Collisions of orbiting ions effectively increase the ion flux collected by the particle, thereby increasing its potential to more positive values. Electron and ion momentum transfer and collection cross sections for scattering from the dust particle are presented.

The contamination of rf glow discharges for microelectronics fabrication by particulates ("dust") is an acknowledged problem due to both contamination of the product and perturbation of the plasma properties.[1–18] Particles (10 s of nm–10 s of μm in size) generally negatively charge in plasmas and usually accumulate at the boundary between the sheath and the bulk plasma in low pressure ($<$ a few Torr) rf glow discharges.[1–11] The accumulation of dust particles at these locations occurs when the dust particles become trapped in quasi-dc potential wells adjacent to the wafer.[12] The wells are formed where two opposing forces balance.[11] The first force is a viscous ion drag which largely consists of elastic collisions between the dust and positive ions in which the ion performs an open orbit "looping" around the dust particle. Conservation of momentum results in accelerating the dust particle in the original direction of the ion.[13] The second force is electrostatic repulsion by the large electric fields in the sheath which forces the dust particle toward the center of the plasma. Observed two-dimensional distributions of dust particles may result from electrostatic traps formed by the nonplanar relief of the surface. Additional effects such as thermophoresis and polarization forces may also influence the transport of particles.[4,6,10,16] Electron transport coefficients are also affected by dust particles due to the large momentum transfer cross sections represented by the geometrical obscuration of the charged dust particles and their shielding. Electron impact rate coefficients for high threshold events decrease due to momentum transfer occurring during electron-dust collisions.[17,18]

The transport of dust particles, and the perturbation of electron and ion swarm parameters depend on the details of the sheath surrounding the dust particles. All of these effects roughly scale as $(r_d+\lambda)^2$, where r_d is the radius of the dust particle and λ is the shielding length. To investigate electron-dust particle and ion-dust particle interactions, a pseudoparticle-in-cell simulation (PICS) has been developed to self-consistently calculate the sheath structure around dust particles. (To avoid confusion, particulate contamination will be called "dust particles" while numerical particles in the PICS will be called pseudoparticles.)

The model will be briefly described. Before executing the PICS, Monte Carlo simulations (MCS) of both the electron and ion swarms are performed using a specified and spatially uniform E/N (electron field/gas number density). The purpose of performing the MCS is to obtain the quasi-steady-state electron and ion energy distributions for use as initial conditions in the PICS. The details of the MCS are described in Ref. 19. All pertinent elastic and inelastic collisions of electrons and ions with the neutral gas, argon in this study, are included in the MCS. The sources of our electron impact cross sections are listed in Ref. 19. The ion collisions include elastic (ion neutral) and charge exchange (ion neutral), with cross sections derived from swarm data,[20] and elastic Coulomb (ion-ion).

After the electron and ion energy distributions are obtained, an uncharged spherical dust particle is introduced into the center of the computational volume. The PICS is then performed while including all of the collision processes described above and simultaneously solving Poisson's equation in the vicinity of the dust particle. Poisson's equation is solved in spherical coordinates in a subvolume centered on the dust particle. The spherical subvolume is centered in a larger rectangular space to which periodic boundary conditions are applied. The potential boundary condition on the outer surface is obtained from the voltage drop resulting from the externally applied E/N. Pseudoparticles striking the dust particle are collected with unity efficiency. The collected charge was averaged over the surface of the dust particle. The surface charge density provides a boundary condition in the form of the electric field at the surface. The PICS is integrated forward in time until the net charge on the dust particle, Q, reaches a steady state. As an alternate method of solution, we began the PICS with an estimated Q, and the PICS was executed to obtain dQ/dt. Based on the sign of dQ/dt, the PICS is repeated with different values of Q to search for the value of Q which yields $dQ/dt=0$.

At the end of the simulation, cross sections for electron and ion momentum transfer to the dust particle by open orbits and by collection by the dust particle are calculated using molecular dynamics (MD) techniques. Electron and ion pseudoparticles are launched into the computational volume with varying impact parameters. The change in momentum and number of pseudoparticles as they leave the volume are summed to calculate the momentum trans-

 0003-6951/93/182197-03$06.00

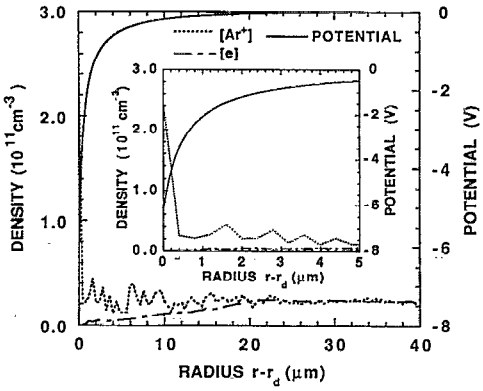

FIG. 1. Calculated electron and ion densities, and plasma potential for a 1-μm-diam dust particle with a bulk plasma density of 2×10^{10} cm^{-3}. The ion and electron densities are the average of 10 snapshots of the pseudoparticle distributions. The inset shows a smoothed expanded view of the region near the particle.

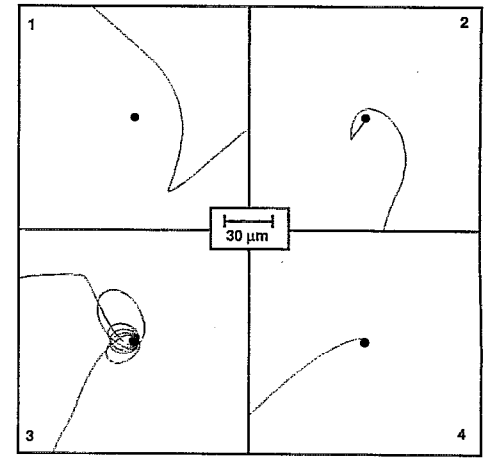

FIG. 2. A selection of ion trajectories around a 5 μm dust particle. These plots are two-dimensional projections of three-dimensional trajectories.

fer and capture cross sections. To isolate the interaction of the electrons or ions with the dust particle, we do not include collisions with the gas during the MD calculations. The collection cross section is therefore a lower limit since some ions are collected following collisions.

The quasi-dc electric potential, and charged particle densities (average of 10 "snapshots") as a function of position are shown in Fig. 1. The Ar gas pressure is 0.2 Torr, and the electron and ion temperatures far from the dust particle are 3.8 and 0.03 eV, respectively. The bulk plasma density far from the dust particle is 2×10^{10} cm^{-3}. Electrons are quickly collected after introducing the dust particle. The initial rate of charge collection is $\simeq -10q$ ns^{-1}. As the sheath forms, the less mobile ions begin to be collected. As Q reaches a steady state, the rate of charging slows. The steady state Q is $\simeq -2364q$ which occurs after $\simeq 100s$ ns, and develops a particle potential of -6.1 V. The charging time decreases with increasing plasma density ($-70q$ ns^{-1} at 2×10^{11} cm^{-3}) and decreasing T_e.

The shielding length (distance to 0.1 of particle potential) around the dust particle for the conditions in Fig. 1 is $\simeq 4.0$ μm. The electron and ion Debye lengths are 103 and 9.2 μm, respectively, and the linearized Debye length is 12.8 μm. λ is therefore approximately 0.3 of the linearized Debye length. The particle potential is approximately equal to 1.6 T_e which is slightly smaller than the potential predicted by collisionless probe theory.[21,22] This result, as well as the deviation of the plasma potential from the Debye–Huckle form,[21] can be partly attributed to the non-Maxwellian "cutoff" electron distribution which is depleted of high energy electrons and nonmonoenergetic incident ions; but is most likely attributed to trapped ion orbits, as discussed below.

For a bulk plasma density of 2×10^{11} cm^{-3}, the calculated charge on the particle fluctuates with an amplitude of $\simeq 20q$. We found for the range of bulk plasma densities examined (10^{10} cm^{-3}–2×10^{11} cm^{-3}) this amplitude is close to the statistical fluctuation in the number of ions in the shielding volume based on the bulk ion density $[(4\pi\lambda^3 n_I/3)^{1/2}]$. For the plasma densities and volumes of interest, each pseudoparticle in the PICS represents a single electron or ion. Although PICS are themselves approximations since the charge density is averaged over a computational cell and there is a noise component to the simulation, the one-to-one correspondence of pseudoparticles and ions (electrons) used in the simulation nevertheless allows one to estimate the statistical fluctuations in the charging of small dust particles in low density plasmas.

The ion density in the vicinity of the dust particle increases while the electron density decreases. The increase in the ion density results from closed and open orbits of ions around the dust particle.[21,23,24] The increase in ion density around the dust particle decreases as r_d/λ increases and as the orbital component of the ion trajectories decreases. A selection of open, closed, and terminal ion orbits around the dust particle are shown in Fig. 2. (These figures are two-dimensional projections of three-dimensional trajectories.) The open orbits are roughly hyperbolic, as shown by trajectories 1 and 2. In trajectory 1, the exiting ion undergoes a collision which redirects its orbit away from the dust particle. In trajectory 2, the exiting ion undergoes a charge exchange collision which allows the thermal ion to be collected. In trajectory 3, the incoming ion undergoes a collision, which allows it to fall into a closed orbit. It undergoes 4 orbits, after which a second collision "kicks" it into an open orbit. Trajectory 4 is a direct collection. Similar orbital motion has been observed in calculations by Goree.[23]

For these conditions, many of the ions which are collected by the dust particle follow a collision. At high bulk plasma densities ($> 10^{11}$ cm^{-3}), the ion density near the dust particle is large enough that ion-ion collisions become important. These collisions allow more ions to drop into closed orbits and allow more ions to be collected by the dust particle. This effectively increases the flux of ions to the dust particle and increases the potential of the dust particle. The potential of the dust particle increased by a few tenths of a volt when including ion-ion collisions.

Cross sections for electron and ion interactions with dust particles (momentum transfer and collection) ob-

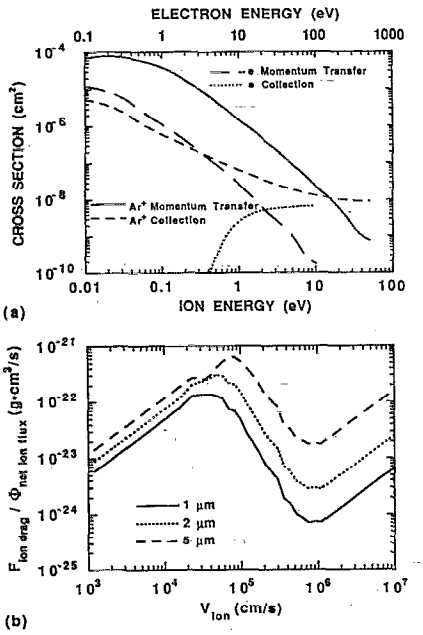

FIG. 3. Calculated momentum transfer properties. (a) Momentum transfer and collection cross sections for electrons and ions (1 μm dust particle, bulk plasma density 3×10^{10} cm^{-3}). (b) The net force on dust particles of various sizes as a function of incident Ar ion velocity. The force is normalized by the net ion flux (cm^{-2} s^{-1}) passing by the dust particle.

tained from the MD simulation are shown in Fig. 3(a) for a bulk plasma density of 3×10^{10} cm^{-3}. Electrons and ions which were collected by the dust particle were excluded from the calculation of the momentum transfer cross section (MTXS), as is accepted practice in swarm studies. The ion and electron MTXS decrease with increasing energy, as does the ion collection cross section (CXS). The electron CXS is zero at energies below the particle potential and increases with increasing energy as only electrons with an energy greater than the particle potential can be collected. The asymptotic values of both the electron and ion CXS are the geometric cross-sectional area of the dust particle (7.9×10^{-9} cm^2).

By combining the ion MTXS and CXS, the drag force on the dust particle due to Ar ions can be calculated. This force is shown in Fig. 3(b). The force is normalized by the net flux of ions passing the dust particle. The increase in the force at low velocities results from the increase in ion momentum while the MTXS is fairly constant. The decrease in the force results from a more rapid decrease in the MTXS than increase in momentum of the ion. Finally, when the MXTS falls below the CXS, the force increases with increasing ion momentum. The ion drag force increases with increasing size of the dust particle since r_d/λ increases. The direct collection component of the force increases and begins at lower velocities with increasing particle size. This shape for the ion drag force was previously analytically predicted by Barnes *et al.*[13]

In conclusion, a model has been developed for the shielding of dust particles in low pressure glow discharges (0.2 Torr Ar, 10^{10}–10^{11} cm^{-3} bulk plasma density). We found that the charging cycle of the dust particle is 10s–to hundreds of ns, which is commensurate with the rf period of plasma processing discharges. The shielding distance can be approximate by the linearized Debye length.[21] Collisions of ions in the vicinity of the dust particle result in closed orbits of the ions and increased collection of ions by the particle, resulting in a more positive potential on the dust particle.

The authors would like to thank M. Barnes, J. Goree, D. Graves, J. Keller, and G. Selwyn for discussions on dust particles dynamics in plasmas. This work was supported by the National Science Foundation (CTS91-13215, ECS91-02326), IBM East Fishkill Facility, the Semiconductor Research Corporation, and the University of Wisconsin ERC for Plasma Aided Manufacturing.

[1] G. S. Selwyn, J. E. Heidenreich, and K. L. Haller, Appl. Phys. Lett. **57**, 1876 (1990).
[2] G. S. Selwyn, J. Singh, and R. S. Bennett, J. Vac. Sci. Technol. A **7**, 2758 (1989).
[3] R. M. Roth, K. G. Spears, G. D. Stein, and G. Wong, Appl. Phys. Lett. **46**, 235 (1985).
[4] G. M. Jellum and D. B. Graves, J. Appl. Phys. **67**, 6490 (1990).
[5] K. Spears, T. M. Robinson, and R. Roth, IEEE Trans. Plasma Sci. **PS-14**, 179 (1986).
[6] G. M. Jellum and D. B. Graves, Appl. Phys. Lett. **57**, 2077 (1990).
[7] K. G. Spears, R. P. Kampf, and T. J. Robinson, J. Phys. Chem. **92**, 5297 (1988).
[8] G. S. Selwyn, J. S. McKillop, K. L. Haller, and J. J. Wu, J. Vac. Sci. Technol. A **8**, 1726 (1990).
[9] J. A. O'Neill, J. Singh, and G. S. Gifford, J. Vac. Sci. Technol. A **8**, 1715 (1990).
[10] G. M. Jellum, J. E. Daugherty, and D. B. Graves, J. Appl. Phys. **69**, 6923 (1991).
[11] T. J. Sommerer, M. S. Barnes, J. H. Keller, M. J. McCaughey, and M. J. Kushner, Appl. Phys. Lett. **59**, 638 (1991).
[12] R. N. Carlile, S. Geha, J. O'Hanlon, and J. Stewart, Appl. Phys. Lett. **59**, 1167 (1991).
[13] M. S. Barnes, J. H. Keller, J. C. Forster, J. A. O'Neill, and D. K. Coultas, Phys. Rev. Lett. **68**, 313 (1992).
[14] Y. Watanabe, M. Shiratani, and H. Makino, Appl. Phys. Lett. **57**, 1616 (1990).
[15] W. J. Woo and Ch. Steinbruchel, Appl. Phys. Lett. **60**, 1073 (1992).
[16] L. Boufendi, A. Plain, J. Ph. Blondeau, A. Bouchoule, C. Laure, and M. Toogood, Appl. Phys. Lett. **60**, 169 (1992).
[17] M. J. McCaughey and M. J. Kushner, Appl. Phys. Lett. **55**, 951 (1989).
[18] M. J. McCaughey and M. J. Kushner, J. Appl. Phys. **69**, 6952 (1991).
[19] Y. Weng and M. J. Kushner, Phys. Rev. A **42**, 6192 (1992).
[20] See, for example, A. V. Phelps, J. Phys. Chem. Ref. Data **20**, 557 (1991).
[21] J. E. Daugherty, R. K. Porteous, M. D. Kilgore, and D. B. Graves, J. Appl. Phys. **72**, 3934 (1992).
[22] J. G. Laframboise, University of Toronto Institute for Aerospace Studies, Report No. 100, 1966.
[23] J. Goree, Phys. Rev. Lett. **69**, 277 (1992).
[24] J. P. Boeuf, Phys. Rev. A **46**, 7910 (1992).